ACS APPLIED MATERIALS & INTERFACES

Research Article

Cite This: ACS Appl. Mater. Interfaces 2017, 9, 44173−44180

www.acsami.org

Evidence for Chemical and Electronic Nonuniformities in the Formation of the Interface of RbF-Treated Cu(In,Ga)Se_2 with CdS

Nicoleta Nicoara,*[,†] Thomas Kunze,[‡] Philip Jackson,[§] Dimitrios Hariskos,[§] Roberto Félix Duarte,[‡] Regan G. Wilks,[‡,∥] Wolfram Witte,[§] Marcus Bär,[‡,∥,⊥] and Sascha Sadewasser[†]

[†]International Iberian Nanotechnology Laboratory (INL), 4715-330 Braga, Portugal

[‡]Renewable Energy, Helmholtz-Zentrum Berlin für Materialien und Energie GmbH (HZB), 14109 Berlin, Germany

[§]Zentrum für Sonnenenergie-und Wasserstoff-Forschung Baden-Württemberg (ZSW), 70563 Stuttgart, Germany

[∥]Energy Materials In-Situ Laboratory Berlin (EMIL), Helmholtz-Zentrum Berlin für Materialien und Energie GmbH, 12489 Berlin, Germany

[⊥]Institut für Physik, Brandenburgische Technische Universität Cottbus-Senftenberg, 03046 Cottbus, Germany

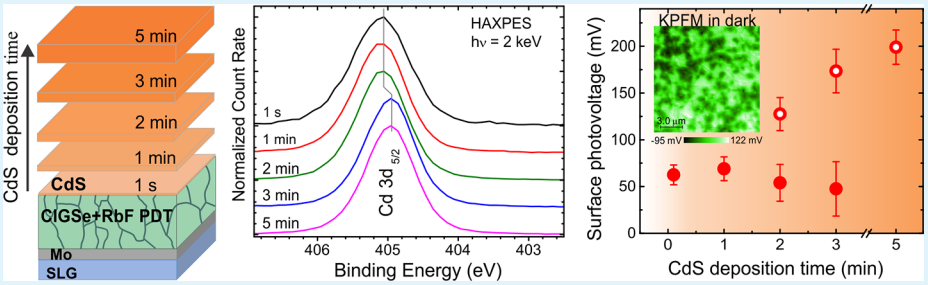

ABSTRACT: We report on the initial stages of CdS buffer layer formation on Cu(In,Ga)Se_2 (CIGSe) thin-film solar cell absorbers subjected to rubidium fluoride (RbF) postdeposition treatment (PDT). A detailed characterization of the CIGSe/CdS interface for different chemical bath deposition (CBD) times of the CdS layer is obtained from spatially resolved atomic and Kelvin probe force microscopy and laterally integrating X-ray spectroscopies. The observed spatial inhomogeneity in the interface's structural, chemical, and electronic properties of samples undergoing up to 3 min of CBD treatments is indicative of a complex interface formation including an incomplete coverage and/or nonuniform composition of the buffer layer. It is expected that this result impacts solar cell performance, in particular when reducing the CdS layer thickness (e.g., in an attempt to increase the collection in the ultraviolet wavelength region). Our work provides important findings on the absorber/buffer interface formation and reveals the underlying mechanism for limitations in the reduction of the CdS thickness, even when an alkali PDT is applied to the CIGSe absorber.

KEYWORDS: *chalcopyrite, thin-film solar cells, alkali fluoride postdeposition treatments, Kelvin probe force microscopy, surface photovoltage, photoelectron spectroscopy*

INTRODUCTION

Recent improvements in the efficiency of Cu(In,Ga)Se_2 (CIGSe) based thin-film solar cells have been obtained with alkali fluoride postdeposition treatments (PDT).[1] It has been reported that this process beneficially modifies the optoelectronic properties of the CIGSe absorber (surfaces),[2,3] providing an improved surface for subsequent buffer layer deposition. Moreover, it has been shown that the alkali PDT allows for a reduction in the required buffer thickness, as compared to non-PDT interfaces—to some extent without significant losses in device performance.[4] Reduction of the buffer thickness is significant for production at an industrial level, where material savings, waste reduction, and cost savings are important issues. This is, in particular, true for a wet-chemical process (e.g., chemical bath deposition, CBD—the standard deposition method of the buffer layer for CIGSe solar cells) of a heavy-metal compound (e.g., CdS, the commonly used buffer layer). In addition, thinner CdS layers would result in an enhanced current collection in the ultraviolet wavelength region leading to gains in the short-circuit current density. However, an exceedingly reduced buffer layer thickness could also result in an "unprotected" absorber/buffer interface that would be more susceptible to modifications, due to air exposure or subsequent deposition steps. Moreover, variations in the layer uniformity, particularly with respect to coverage or composition could have an impact on cell performance. In the first case, this would result in pinholes that could lead to shunt paths enhancing the recombination current and thus decreasing efficiency.[5] In the second case, there would be a complicated interface structure (also in view of the band energy level alignment) that could

Received: August 18, 2017
Accepted: November 27, 2017
Published: November 27, 2017

DOI: 10.1021/acsami.7b12448
ACS Appl. Mater. Interfaces 2017, 9, 44173−44180

either lead to the formation of beneficial point contacts between absorber and emitter or that could also open up detrimental shunt paths. It has been empirically shown that short CBD times lead to the formation of inhomogeneous CdS layers, which have been attributed to the chemical reaction mechanisms in the CBD that differed depending on the orientation, polarity, composition, and/or surface energetics of the CIGSe grains.[6] As reported previously, CBD grown CdS plays an important role in establishing a favorable band alignment[7−9] and improvement of the lattice mismatch at the interface.[10] Furthermore, during the CBD process, the CIGSe surface is cleaned, thus preconditioning the absorber to form a defect-poor interface to the buffer layer.[11] Basic knowledge related to the chemical and electronic properties of CIGSe/CdS interfaces has been gained previously,[12−14] but many aspects related to the CdS growth mechanism and its effect on the interface quality, especially for CIGSe subjected to an alkali PDT,[15−18] are still not well understood, in particular taking spatial inhomogeneities into consideration.[19,20] In this work, we investigate the early stages of the CdS growth on RbF-PDT CIGSe absorbers, which result in efficiencies around 20% (w/ ARC) for related reference cells, by a combination of spatially resolved and integrating techniques. Several samples, with CBD treatment times varying between 1 s and 5 min, are investigated by atomic (AFM) and Kelvin probe (KPFM) force microscopy, hard X-ray photoelectron spectroscopy (HAXPES), and soft X-ray emission spectroscopy (XES). The spatially resolved topography and surface potential obtained with AFM and KPFM and the laterally integrated near-surface chemical structure obtained with HAXPES and XES allow us to analyze the evolution of the interface properties as a function of CdS buffer thickness.

EXPERIMENTAL SECTION

Two sets of CIGSe absorbers were deposited in a multistage process onto Mo-coated soda-lime glass (SLG) substrates following the ZSW standard procedure for high-efficiency CIGSe solar cell manufacturing.[1] An alkali PDT using RbF was performed after the CIGSe process, employing a procedure similar to that described in ref 4. Buffer layers with different thicknesses were deposited by dipping the sample in a standard CdS bath solution[21] for times varying between 1 s and 5 min. After a short nucleation period, the initial growth of CdS takes place within the first minute(s). Buffer layers used for solar cells reach up to 50 nm in thickness after 8−10 min in the CBD. We note that respective reference solar cells reach efficiencies around 20% (w/ ARC). One thickness series was sent to INL for AFM/KPFM studies, and the other set was sent to HZB for HAXPES/XES measurements. To minimize surface contamination, all samples were sealed and packed in an N_2 environment directly after preparation. For the HAXPES measurements, significant effort has been made to avoid air exposure by mounting the samples in an inert N_2 atmosphere and by transferring them into the endstation loadlock using a N_2-purged glovebag. Unfortunately, this was not possible for KPFM and XES measurements. The air exposure during their mounting was minimized to 10 and 30 min, respectively, before entering the ultrahigh vacuum (UHV) systems for measurements.

Synchrotron-based HAXPES measurements with an excitation energy of 2003 eV (henceforth called 2 keV) were carried out at the HiKE endstation[22] located at HZB's BESSY II KMC-1 beamline.[23] The HiKE endstation is equipped with a Scienta R4000 hemispherical electron energy analyzer. The excitation from the beamline and the measurement axis of the analyzer are at right angles, with the polarization vector of the photons aligned with the analyzer; measurements were performed in near-grazing incidence. The samples were not exposed to air before the measurements. The base pressure of the endstation was $<10^{-8}$ mbar. A pass energy of 200 eV was used for all measurements, and the excitation energy was calibrated by measuring Au 4f spectra of a clean, electrically grounded Au foil and setting the Au $4f_{7/2}$ binding energy to 84.00 eV.[24] Spectra were recorded using the first diffraction order of the Si(111) double crystal monochromator (DCM) pair, providing combined (analyzer plus X-ray line width) energy resolution of approximately 0.25 eV. Core level intensities were derived by simultaneous fit of the peaks using Voigt profiles and a linear background.

Synchrotron-based soft X-ray emission spectroscopy (XES) was performed in the soft X-ray fluorescence (SXF) endstation[25] of beamline 8.0.1 at the Advanced Light Source (Lawrence Berkeley National Laboratory, Berkeley, CA, U.S.A.). In this setup, the excitation and emission are at right angles, with the excitation photon polarization vector aligned with the spectrometer entrance slit; the samples were angled such that incoming and outgoing photons were at 45° to the sample surface. The base pressure of the endstation was $<5 \times 10^{-9}$ mbar. The samples were transferred into the chamber after only a brief air exposure. Photon energies of 200 eV were used as excitation for S $L_{2,3}$ measurements. The XES energy scale was calibrated based on measurements of CdS reference spectra.[26]

KPFM measurements were carried out in an UHV (base pressure $<10^{-10}$ mbar) scanning probe microscope (Omicron Nanotechnology GmbH), controlled by a Nanonis controller (SPECS Zurich GmbH), and using Pt/Ir-coated cantilevers (PPP-NCHPt-Nanosensors) with f_0 = 169.131 kHz. The amplitude modulation (AM) KPFM technique was used for the detection of the contact potential difference (CPD) with an applied bias V_{AC} = 300 mV tuned at the second oscillation mode of the cantilever (f_1 = 1.049.275 MHz). The oscillating electrostatic forces are minimized by applying a compensating voltage (V_{DC}) to the tip. The CPD is defined as the work function (Φ) difference between sample and tip: $V_{CPD} = -V_{DC} = e(\Phi_{sample} - \Phi_{tip})$. The same tip was used for all reported measurements to ensure comparability of the CPD values between the measurements. To determine the surface photovoltage (i.e., the change in CPD with illumination), we used a laser diode (λ = 635 nm) at an intensity of approximately 100 mW/cm^2, with an illumination angle of 28° to the normal, to ensure illumination of the sample under the tip and cantilever beam.

For large area scans, we used a Bruker Dimension Icon AFM under ambient conditions. The same type of sensors as previously mentioned were used. Sample topography and CPD are acquired using the dual-pass technique. In the first pass, a scan line of the topography is recorded using tapping mode. In the second pass, the tip is lifted at a constant distance from the sample surface (lift height ≈ 5 nm), and the same scan line is recorded in AM-KPFM, during which an AC bias voltage (V_{AC} = 500 mV) is applied to the tip at the mechanical resonance f_0 of the cantilever.

The KPFM data analysis procedure is illustrated in Figure 1. From the CPD image (b), which is acquired simultaneously with the topography (a), the CPD distribution is plotted as a histogram[27] (d). From such histograms, we determine the maximum CPD value and the width of the potential distribution at 1/e of the counts at the maximum (i.e., for the CPD_{dark}, left histogram, we find a maximum at CPD = −62 mV and a width of ∼60 mV). The width is then plotted as error bars. To determine the surface photovoltage (SPV), the same area is scanned again under illumination (Figure 1c). From a pair of CPD images in the dark and under illumination, the SPV is calculated according to $SPV = CPD_{illum.} - CPD_{dark}$.[27] In this case, we obtained an SPV ∼ 60 mV.

RESULTS

Figure 2a shows the Cd $3d_{5/2}$ core level photoemission measured by HAXPES as a function of the CdS CBD time. A clear Cd signal is already detectable from the 1 s CBD CIGSe/CdS sample on. For longer deposition times, the intensity increases significantly (see stated magnification factors). The fwhm of the peak decreases with increasing CBD time (inset of Figure 2a). There are observable differences between short CBD times (1 s, 1 min, and 2 min) compared to long CBD

DOI: 10.1021/acsami.7b12448
ACS Appl. Mater. Interfaces 2017, 9, 44173−44180

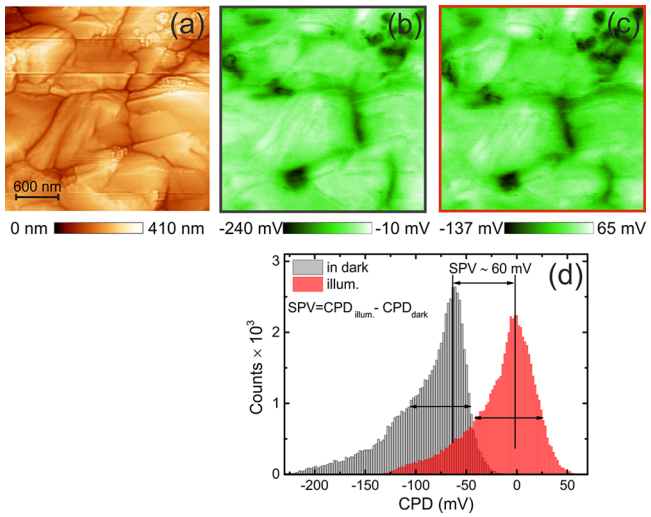

Figure 1. (a) AFM topography and KPFM data (CPD maps) in (b) the dark and (c) under illumination, acquired in the same region of a CIGSe sample with RbF and 1 s CBD CdS. (d) Histogram analysis of CPD maps in (b) and (c). See text for details.

times (3 and 5 min): the fwhm of the peak decreases over the short CBD times (indicating that multiple Cd species are present in these samples), approaching a constant value of 0.85 eV for the 3 and 5 min samples. Also, there is a shift in the Cd $3d_{5/2}$ peak position (−0.13 ± 0.02) eV between the short and long deposition times. These findings indicate that the composition of the CdS buffer remains constant after ∼3 min of CBD time, while the spectra of the short CBD time samples provide information about the formation of the CIGSe/CdS interface. Figure 2b depicts the region of the S 2s, Rb 3p, and Se 3s core levels. Note that we observed no F signal on the absorber, and thus, on the basis of our findings on the chemical structure of NaF/KF-PDT CIGSe absorbers,[28] we presume that Rb is most likely incorporated into the upper region of the CIGSe absorber rather than being present in the form of RbF. After correcting the Rb 3p and Se 3s line intensities by the corresponding photoionization cross sections, we calculate a Rb:Se ratio of 0.07:1.00 [±0.03] for the CIGSe/CdS 1 s sample. The attenuation of the Rb 3p as a function of CBD time is similar to that of the Se 3s signal, indicating that the Rb is not removed in the chemical bath. The decrease in Rb 3p and Se 3s intensity, together with the increasing S 2s signal with CBD time, is in agreement with the deposition of the buffer layer.

To estimate the thickness of the CdS buffer layer, the inelastic mean free path (IMFP) of the photoelectrons is considered. The substrate HAXPES signal intensity (I) is attenuated exponentially due to the covering buffer layer according to $I = I_0 \times \exp(-z/\mathrm{IMFP})$, with I_0 being the intensity of the bare, uncovered substrate, and z being the thickness of the covering layer. If z reaches 3 × IMFP, the substrate signal is reduced to 5% of I_0. Therefore, we estimate the information depth of our measurement to be approximately 3 × IMFP. The IMFP of the electrons originated from the absorber core level with the highest photoionization cross section- In 3d- in CdS is around 3 nm.[29,30] Considering that this substrate peak cannot be observed for the CIGSe/CdS 3 min sample (not shown), we estimate the minimum thickness for the buffer layer deposited within 3 min to be approximately 9 nm. Note that for this estimation, a homogeneous buffer layer, completely covering the CIGSe absorber, is assumed. As it will be discussed below, significant topographical inhomogeneities are observed for the CIGSe/CdS samples, and thus, the derived minimum thickness has to be considered an effective value averaged over different sample structures.

However, while we can observe a clear Cd $3d_{5/2}$ signal for the CIGSe/CdS 1 s sample (see Figure 2a), no corresponding S 2s signal can be clearly observed. The complexity of the chemical (interface) structure is also seen in the HAXPES-derived Cd:S

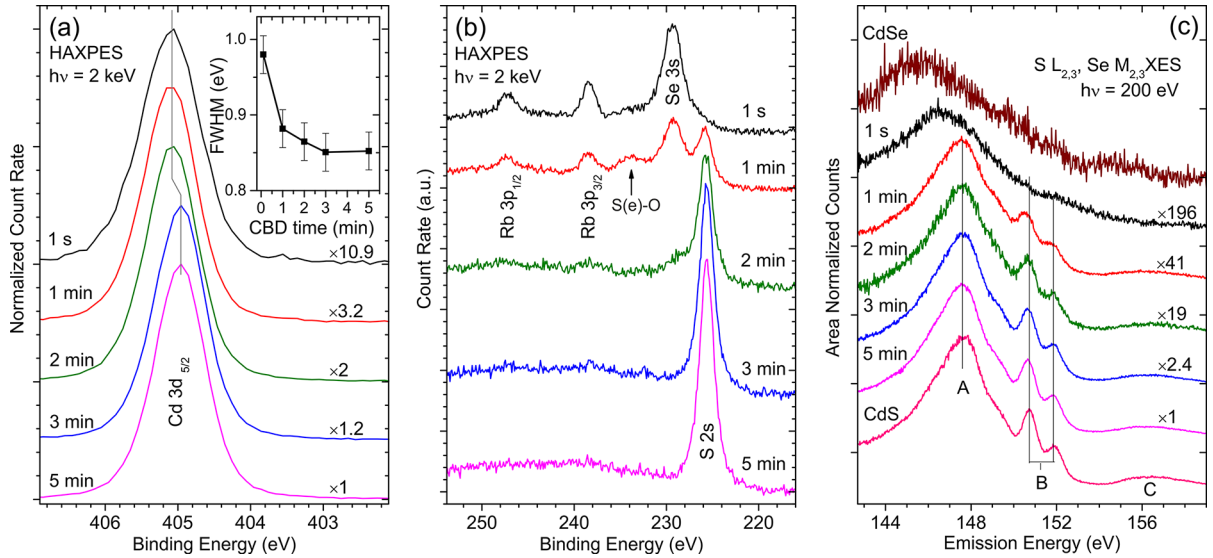

Figure 2. (a) Normalized HAXPES Cd $3d_{5/2}$ core level lines as a function of the chemical bath deposition time. The given magnification factors indicate the changes in relative intensity. The inset shows the fwhm as a function of the CBD time. (b) Binding energy region of the Rb 3p, Se 3s, and S 2s core levels for different CBD times. The arrow indicates a chemical shift of the Se 3s and/or the S 2s line to higher binding energies ascribed to Se−O and/or S−O bonds. (c) Area-normalized S $L_{2,3}$ (Se $M_{2,3}$) XES spectra of the CIGSe/CdS series together with reference spectra of CdSe and CdS powder samples. The given magnification factors state the relative intensity evolution, and the labels A−C indicate spectral features of CdS as described in the text in detail. Vertical offsets between the spectra are added in each panel for clarity.

DOI: 10.1021/acsami.7b12448
ACS Appl. Mater. Interfaces 2017, 9, 44173−44180

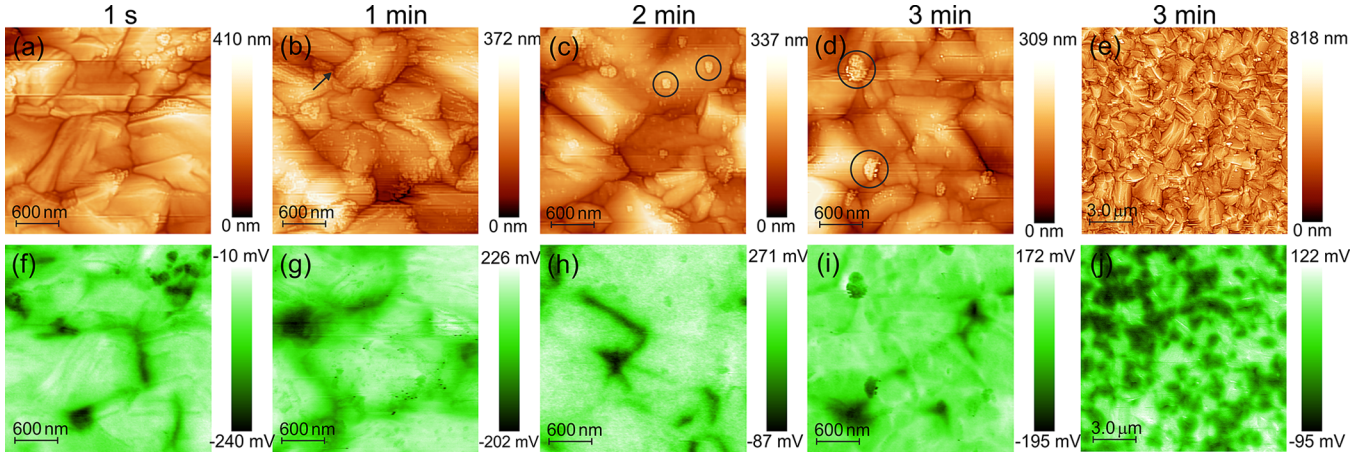

Figure 3. AFM and KPFM of the RbF-PDT CIGSe surface after various CdS deposition times: (a) 1 s, (b) 1 min, (c) 2 min, (d,e) 3 min of CBD. The top row shows derivative-enhanced views of the topography, and the bottom row (f–j) shows the simultaneously acquired contact potential difference (CPD) maps in the dark. Images size: (a–d) 3 μm × 3 μm, (e) 15 μm × 15 μm. Note that (e) and (j) were acquired in an ambient-AFM setup.

ratio, which after taking the photoionization cross section, inelastic mean free path, and transmission function of the analyzer into account is determined to be around 3:1 for all samples deposited employing CBD times longer than 1 min, indicating that the buffer is not a stoichiometric CdS. Significant spectral intensity of O 1s and C 1s lines (not shown) can be detected on all samples. Thus, we propose that substantial amounts of O and/or C are incorporated into the buffer (rather than being exclusively attributed to a surface contamination layer). The employed sulfur source (thiourea) that decomposes during the CBD process releasing "free" sulfur ions leaves behind different carbon decomposition products, which might explain the incorporation of carbon into the buffer layer. Oxygen is available in the form of hydroxides in the aqueous ammonia containing CBD solution, opening a route of incorporating oxygen into CdS. Note that the formation of Cd(S,O) films in chemical baths has been reported recently[31] and is to some extent in agreement with the HAXPES-derived Cd, S, and O sample contents. It has been shown[31] that the incorporation of oxygen into the CdS buffer layer increases transparency and thus could benefit solar cell performance. In addition, we do find some evidence for the presence of Se–O bonds and/or S–O bonds in the form of SeO_x^{2-} with $x \geq 3$ and SO_4^{2-}, respectively, as indicated by the arrow in Figure 2b for short CBD times. Furthermore, C–O bonds (additional contributions to the C 1s peak—not shown—at 288 eV) are observed for all samples. Cd diffusion into the upper region of the absorber and/or the formation of Cd–Se bonds close to the interface could indicate a further deviation from the expected buffer stoichiometry in the interface region.

As a further probe of the (local) chemical structure of the CIGSe/CdS interface—here from the particular viewpoint of the sulfur—S $L_{2,3}$/Se $M_{2,3}$ XES measurements were performed and are displayed in Figure 2c. Similar to the overlapping S and Se core level photoemission signals shown in Figure 2b, the S $L_{2,3}$ and Se $M_{2,3}$ emission signals also overlap, complicating analysis. However, the transition matrix element for the Se $M_{2,3}$ emission (i.e., emission caused by fluorescence decay into the Se 3p core holes) is several orders of magnitude smaller than the analogous S $L_{2,3}$ matrix element, making the measurements significantly more sensitive to sulfur. As indicated by the decreasing magnification factors that were used in the intensity normalization, the spectral intensity drastically increases with CBD time and thus with S content of the probed samples. Note that the enhanced bulk sensitivity of XES compared to the 2 keV HAXPES information depth may explain the different magnification factors. The spectra of the CIGSe/CdS 1–5 min samples are in good agreement with that of the CdS powder reference showing all related spectral features ascribed to (A) S 3s, (B) Cd 4d, and (C) upper valence-band-derived states decaying into the spin–orbit split S 2p core holes.[32] In particular, feature (B) is direct evidence for the formation of S–Cd bonds, i.e., all present/deposited sulfur is exclusively bound to Cd for these samples. However, the absence of feature (B) from the spectrum of the CIGSe/CdS 1 s sample (together with the significantly reduced intensity and the broadening and shift to lower emission energies of feature (A) is a further indication that no S–Cd bonds are formed at the beginning of the CBD process, in agreement with the absence of a S signal in the corresponding HAXPES data (Figure 2b). Note that no indication for SO_4^{2-} bonds, which would lead to a pronounced double peak around 155 eV induced by S 3s-derived states and a peak at 161 eV induced by a S 3d-derived state,[33] is observed in the XES spectra. Therefore, the observation of the spectral signature in the HAXPES data around a binding energy of 234 eV (see Figure 2b) and its tentative attribution to Se–O and/or S–O bonds suggests that SO_4^{2-} is formed exclusively at the sample surface, considering the increased bulk sensitivity of XES (effective attenuation length for S $L_{2,3}$ XES in CdS is approximately 60 nm[34] compared to an IMFP of approximately 3 nm for 2 keV HAXPES measurements) or is present in only negligible amounts.

To shed further light on the solution-growth process of CdS on CIGSe absorber layers subjected to RbF-PDT, we performed spatially resolved AFM and KPFM measurements. Figure 3 shows representative topography and CPD images obtained on CIGSe/CdS with chemical bath deposition times of 1 s and 1, 2, and 3 min, respectively. Topography and corresponding CPD images were taken at different locations, separated by hundreds of micrometers, and a total of ~30 images were analyzed per sample. The top panels show topography displayed in a derivative-enhanced view. To enhance the visibility of small features, the topography image was mixed with its derivative image at a 90/10 ratio. The

DOI: 10.1021/acsami.7b12448
ACS Appl. Mater. Interfaces 2017, 9, 44173–44180

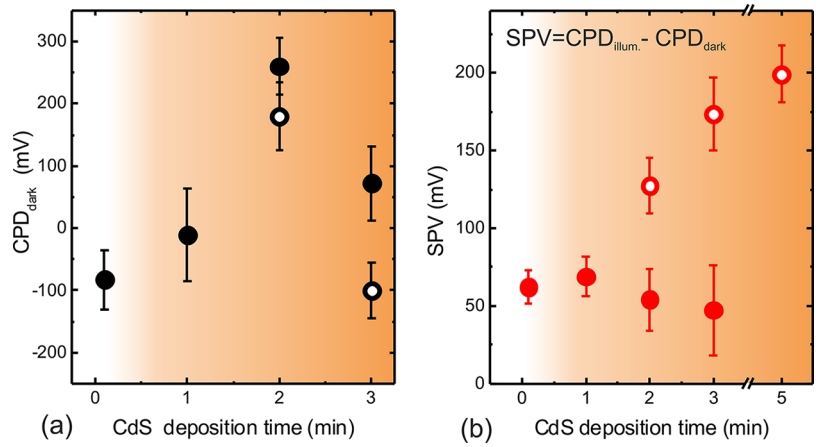

Figure 4. (a) Contact potential difference (CPD) in dark and (b) surface photovoltage (SPV) as a function of CdS CBD time. Homogeneous values are observed for 1 s and 1 min of CdS deposition time. For the samples with 2 and 3 min of CdS deposition time, areas with significantly different CPD values are observed, indicated by open and solid symbols. Here, areas with high CPD correspond to low SPV (solid symbols), and areas showing low CPD exhibit high SPV (open symbols).

surface morphologies displayed in Figure 3a–e are similar in appearance—indicative of the well-known faceted CIGSe.[35] The presence of clusters (as shown in Figure 3a–d) is observed starting with a CBD time of 1 s. The size and density of these clusters increase with CdS deposition time. Their locations appear to be random (they occur both on the grain surface and at grain boundaries), and they exhibit a lower CPD compared to that of cluster-free surface areas.

To quantitatively compare the surface potential as a function of increasing CdS deposition times, we analyze KPFM data measured in ∼30 different 3 μm × 3 μm regions for each sample (Figure 4a). The plotted data represent mean CPD values, and the error bars correspond to the mean CPD variation, determined from the statistical analysis of the CPD histograms. A first observation inferred from the data in Figure 4a is the increase of the CPD up to 2 min of CBD, followed by a significant decrease for the 3 min of CBD sample. Second, the results show uniform CPD values ((−80 ± 48) mV and (−10 ± 75) mV) for samples with 1 s and 1 min of CBD time. However, for samples with 2 and 3 min of CdS deposition, we observe regions with two significantly different CPD values. In case of the 2 min CdS sample, the CPD is either (+180 ± 55) mV or (+260 ± 45) mV, whereas for the CIGSe/CdS 3 min sample, we find images with (−100 ± 45) mV and others with (+70 ± 60) mV (indicated by the open and solid circles, respectively). These inhomogeneities in the CPD data are attributed to a CPD variation on a lateral scale larger than the image size (3 μm × 3 μm). To confirm this hypothesis, larger areas were scanned in another AFM setup operated in ambient conditions; an example is shown in Figure 3e,j for the CIGSe/CdS 3 min sample. A clear CPD gradient can be identified by comparing the top-left corner and the bottom right corner in this 15 μm × 15 μm size region. We note that the KPFM measurements of the sample with 5 min of CdS deposition time were performed with a different tip, and therefore, the CPD value cannot be compared to the other samples. Nevertheless, since the SPV is independent of the tip work function, the SPV of this sample was determined correctly and is presented in Figure 4b.

These inhomogeneities are also apparent in the results obtained under illumination. Figure 4b represents mean SPV values (always determined from pairs of CPD maps measured in the dark and under illumination). The error bars correspond to the SPV standard deviation (less than ∼30 mV). The results show homogeneous SPV values ∼60–70 mV for 1 s and 1 min of CBD and larger values for longer CBD times, with a maximum of ∼200 mV for 5 min of CdS deposition. For the samples with 2 and 3 min of CdS deposition time, similar to the CPD, the SPV also shows two distinct values of ∼50 mV (2 and 3 min of CBD) in some areas and ∼125 mV (2 min of CBD) and ∼175 mV (3 min of CBD) in other areas, respectively. It is important to note that areas with high CPD correspond to areas with low SPV (solid symbols), and areas showing low CPD exhibit high SPV (open symbols).

DISCUSSION

The obtained results show that the formation of the CIGSe/CdS pn-junction requires several minutes in the chemical bath and indicate that complex reactions at the RbF-treated CIGSe surface take place in the first steps (1 s to 1 min) of the CBD process. We observe that within 1 s of CBD, a Cd "adsorption" at the CIGSe surface takes place, as confirmed by the presence of a clear Cd 3d$_{5/2}$ HAXPES signal. The absence of a clear S 2s HAXPES signal and of Cd 4d-derived features in the S L$_{2,3}$ XES data excludes the deposition of CdS from the solution and supports more the formation of Cd–Se bonds in this deposition time regime presumably by chemisorption. This has been previously reported to occur on $CuGaSe_2$ absorbers upon a partial electrolyte treatment (simulating chemical bath conditions without a sulfur source),[36] suggesting that CdSe formation may contribute to the broad Cd 3d$_{5/2}$ lines in the spectra of the short CBD time samples (Figure 2a). The incorporation of C and/or O in the buffer and/or the diffusion of Cd into the upper region of the CIGSe absorber are additional potential scenarios affecting buffer composition also for longer CBD times.

During the initial phase of the buffer deposition (1 s to 2 min of CBD time), an increase of the CPD of ∼200–300 mV is observed by KPFM. This change in work function could be caused by a change in band bending and/or chemical structure. For the same CBD times, the HAXPES Cd 3d$_{5/2}$ peak is centered at higher binding energy and exhibits a wider fwhm compared to longer CBD times. Additionally, a Rb 3p signal is observed for these samples. These observations indicate a

DOI: 10.1021/acsami.7b12448
ACS Appl. Mater. Interfaces 2017, 9, 44173–44180

complex interface formation during this CBD phase resulting in CBD time and thus buffer-thickness-dependent chemical structure changes. We suggest this composition profile as the main reason for the observed CPD change. The proposed formation of CdSe in the interface region may contribute to this complex situation. Further effects that should be considered are the formation of an interface dipole, a Rb-containing absorber surface compound, similar to the K−In−Se type species that has been reported in the case of a KF-PDT CIGSe[17] and/or its CBD-induced conversion into a $CdIn_2Se_4$ compound as proposed by Lepetit.[37] The incorporation of (different amounts of) carbon or oxygen into the buffer (see discussion above) may also play a role.

For longer CBD times (≥3 min), the HAXPES Cd $3d_{5/2}$ peak narrows and shifts to a lower binding energy, and the S $L_{2,3}$ XES data are dominated by S−Cd bonds. Simultaneously, we observe a drop in the CPD, accompanied by significant inhomogeneities. For 2 and 3 min of CBD time, KPFM results clearly indicate that some parts of the sample have high CPD and low SPV values (solid symbols in Figure 4)—this relation is attributed to sample areas with a thin buffer layer of complex composition profiles as described above. In contrast, regions with lower CPD and higher SPV values are also observed. The lower CPD could again be explained by a change in chemical structure and/or band bending. However, the high SPV clearly indicates the formation of a pn-junction, which is also in agreement with the CPD reduction—the simultaneous CPD drop reflects the lower work function as a result of the interface-induced downward band bending in the CIGSe.

The shift in the binding energy of the Cd $3d_{5/2}$ core level line and the reduction of the fwhm also occur at the transition from 2 to 3 min of CBD time. This may be attributed to a changing chemical structure from several buffer components to a single-species buffer (→ CdS). After 3 min of CBD time, HAXPES results further indicate a complete coverage of the absorber with a buffer layer (of an effective thickness >9 nm). Note that in this case and longer CBD times, the absorber is beyond the information depth of the 2 keV HAXPES measurements, and thus, the suggested interface-induced band bending cannot be accessed for the samples (partially) showing high SPV values.

We now turn to the discussion of the clusters observed in the AFM and KPFM images. For the 1 s sample, we attribute these clusters to CdSe-containing agglomerates, in agreement with the presence of Cd and absence of S and S−Cd bonds as revealed by our HAXPES and XES data. Small deposits in the form of clusters have also been observed for short CBD times using scanning electron microscopy imaging.[6] Other studies using energy-dispersive X-ray spectroscopy (EDS) suggest that the CBD process induces a chemical reaction at the chalcopyrite surface which, besides other effects (i.e., surface cleaning), creates CdSe in the form of segregated clusters.[37,38]

For CBD times exceeding the nucleation period of the CBD CdS process, we speculate that these clusters could act as nucleation centers resulting in a preferred deposition of CdS. These clusters alone, however, cannot explain the observed attenuation of the HAXPES absorber signals discussed above, and so, a buffer layer conformally covering the CIGSe absorber must also be formed in the CBD. These CdSe/CdS agglomerates (with a height between 10 and 80 nm, as determined from the AFM topography images) exhibit a lower work function in the CPD images, compared to the surrounding buffer material, independent of CBD time. This might be explained by the presence of sufficient buffer material at these sites that allows the formation of a pn-junction and the corresponding stronger downward band bending.

CONCLUSIONS

Using integrating HAXPES and XES and spatially resolved KPFM, we have analyzed the evolution of the chemical and electronic properties at the interface formed between RbF-PDT CIGSe absorbers and CdS buffer layers during the initial stages of the CBD process. Our results suggest that short CBD times (<2 min) lead to a complex interface region, which is reflected by the presence of multiple (Cd) species and low SPV values. The observed sizable SPV values for CBD times longer than 3 min can be associated with a pn-junction behavior, indicating the formation of a sufficiently thick CdS layer, although some layer inhomogeneity is still observed for 3 min of CBD time. Our findings indicate that although the alkali-PDT of CIGSe favors the use of thinner CdS buffer layers, a CBD time longer than 3 min is required to form a suitable and sufficiently homogeneous junction. Shorter deposition times result in a chemically and electronically inhomogeneous interface structure that might deteriorate device performance, thus confirming empirical observations based on device efficiencies.

AUTHOR INFORMATION

Corresponding Author

*E-mail: nicoleta.nicoara@inl.int (N.N.)

ORCID

Nicoleta Nicoara: 0000-0002-0909-4635

Marcus Bär: 0000-0001-8581-0691

Author Contributions

The manuscript was written through contributions of all authors. All authors have given approval to the final version of the manuscript.

Funding

This project has received funding from the European Union's Horizon 2020 research and innovation program under grant agreement No 641004 (project Sharc25).

Notes

The authors declare no competing financial interest.

ACKNOWLEDGMENTS

We thank HZB for the allocation of synchrotron radiation beamtime for HAXPES measurements. T.K., R.F., R.G.W., and M.B. are grateful to the Impuls- und Vernetzungsfonds of the Helmholtz Association (VH-NG-423). This research used resources of the Advanced Light Source, which is a DOE Office of Science User Facility under contract no. DE-AC02-05CH11231.

REFERENCES

(1) Jackson, P.; Wuerz, R.; Hariskos, D.; Lotter, E.; Witte, W.; Powalla, M. Effects of Heavy Alkali Elements in Cu(In,Ga)Se_2 Solar Cells with Efficiencies up to 22.6%. *Phys. Status Solidi RRL* **2016**, *10*, 583−586.

(2) Laemmle, A.; Wuerz, R.; Powalla, M. Efficiency Enhancement of Cu(In,Ga)Se_2 Thin-Film Solar Cells by a Post-Deposition Treatment with Potassium Fluoride. *Phys. Status Solidi RRL* **2013**, *7*, 631−634.

(3) Pianezzi, F.; Reinhard, P.; Chirila, A.; Bissig, B.; Nishiwaki, S.; Buecheler, S.; Tiwari, A. N. Unveiling the Effects of Post-Deposition Treatment with Different Alkaline Elements on the Electronic Properties of CIGS Thin Film Solar Cells. *Phys. Chem. Chem. Phys.* **2014**, *16*, 8843−8851.

DOI: 10.1021/acsami.7b12448
ACS Appl. Mater. Interfaces 2017, 9, 44173−44180

(4) Chirila, A.; Reinhard, P.; Pianezzi, F.; Bloesch, P.; Uhl, A. R.; Fella, C.; Kranz, L.; Keller, D.; Gretener, C.; Hagendorfer, H.; Jaeger, D.; Erni, R.; Nishiwaki, S.; Buecheler, S.; Tiwari, A. N. Potassium-Induced Surface Modification of $Cu(In,Ga)Se_2$ Thin Films for High-Efficiency Solar Cells. *Nat. Mater.* **2013**, *12*, 1107−1111.
(5) Contreras, M. A.; Romero, M. R.; To, B.; Hasoon, F.; Noufi, R.; Ward, S.; Ramanathan, K. Optimization of CBD CdS Process in High-Efficiency $Cu(In,Ga)Se_2$-based solar cells. *Thin Solid Films* **2002**, *403*−*404*, 204−211.
(6) Witte, W.; Abou-Ras, D.; Hariskos, D. Chemical Bath Deposition of Zn(O,S) and CdS buffers: Influence of $Cu(In,Ga)Se_2$ Grain Orientation. *Appl. Phys. Lett.* **2013**, *102*, 051607−051610.
(7) Schmid, D.; Ruckh, M.; Schock, H. W. A Comprehensive Characterization of the Interfaces in Mo/CIS/CdS/ZnO Solar Cell Structures. *Sol. Energy Mater. Sol. Cells* **1996**, *41-42*, 281−294.
(8) Morkel, M.; Weinhardt, L.; Lohmüller, B.; Heske, C.; Umbach, E.; Riedl, W.; Zweigart, S.; Karg, F. Flat Conduction-Band Alignment at the $CdS/CuInSe_2$ Thin-film Solar-Cell Heterojunction. *Appl. Phys. Lett.* **2001**, *79*, 4482−4484.
(9) Weinhardt, L.; Bär, M.; Muffler, H.-J.; Fischer, Ch.-H.; Lux-Steiner, M. C.; Niesen, T. P.; Karg, F.; Gleim, Th.; Heske, C.; Umbach, E. Impact of Cd^{2+}- Treatment on the Band Alignment at the ILGAR-$ZnO/CuIn(S,Se)_2$ Heterojunction. *Thin Solid Films* **2003**, *431*−*432*, 272−276.
(10) Nakada, T. Nano-Structural Investigations on Cd-doping into $Cu(In,Ga)Se_2$ Thin Films by Chemical Bath Deposition Process. *Thin Solid Films* **2000**, *361*−*362*, 346−352.
(11) Kessler, J.; Ruckh, M.; Hariskos, D.; Rühle, U.; Menner, R.; Schock, H. W. Interface Engineering Between $CuInSe_2$ and ZnO. In *Conf. Rec. 23rd IEEE PVSC*, 1993, 447−452.
(12) Heske, C.; Eich, D.; Fink, R.; Umbach, E.; van Buuren, T.; Bostedt, C.; Terminello, L. J.; Kakar, S.; Grush, M. M.; Callcott, T. A.; et al. Observation of Intermixing at the Buried $CdS/Cu(In, Ga)Se_2$ Thin Film Solar Cell Heterojunction. *Appl. Phys. Lett.* **1999**, *74*, 1451−1453.
(13) Weinhardt, L.; Bär, M.; Pookpanratana, S.; Morkel, M.; Niesen, T. P.; Karg, F.; Ramanathan, K.; Contreras, M. A.; Noufi, R.; Umbach, E.; Heske, C. Sulfur Gradient-Driven Se Diffusion at the $CdS/CuIn(S,Se)_2$ Solar Cell Interface. *Appl. Phys. Lett.* **2010**, *96*, 182102−182104.
(14) Pookpanratana, S.; Repins, I.; Bär, M.; Weinhardt, L.; Zhang, Y.; Félix, R.; Blum, M.; Yang, W.; Heske, C. $CdS/Cu(In,Ga)Se_2$ Interface Formation in High-Efficiency Thin Film Solar Cells. *Appl. Phys. Lett.* **2010**, *97*, 074101−074103.
(15) Pistor, P.; Greiner, D.; Kaufmann, C. A.; Brunken, S.; Gorgoi, M.; Steigert, A.; Calvet, W.; Lauermann, I.; Klenk, R.; Unold, T.; et al. Lux-Steiner M.-C. Experimental Indication for Band Gap Widening of Chalcopyrite Solar Cell Absorbers After Potassium Fluoride Treatment. *Appl. Phys. Lett.* **2014**, *105*, 063901.
(16) Reinhard, P.; Bissig, B.; Pianezzi, F.; Avancini, E.; Hagendorfer, H.; Keller, D.; Fuchs, P.; Döbeli, M.; Vigo, C.; Crivelli, P.; Nishiwaki, S.; Buecheler, S.; Tiwari, A. N. Features of KF and NaF Postdeposition Treatments of $Cu(In,Ga)Se_2$ Absorbers for High Efficiency Thin Film Solar Cells. *Chem. Mater.* **2015**, *27*, 5755−5764.
(17) Handick, E.; Reinhard, P.; Alsmeier, J.-H.; Köhler, L.; Pianezzi, F.; Krause, S.; Gorgoi, M.; Ikenaga, E.; Koch, N.; Wilks, R. G.; Buecheler, S.; Tiwari, A. N.; Bär, M. Potassium Postdeposition Treatment-Induced Band Gap Widening at $Cu(In,Ga)Se_2$ Surfaces − Reason for Performance Leap? *ACS Appl. Mater. Interfaces* **2015**, *7*, 27414−27420.
(18) Nicoara, N.; Lepetit, T.; Arzel, L.; Harel, S.; Barreau, N.; Sadewasser, S. Effect of the KF Post-Deposition Treatment on Grain Boundary Properties in $Cu(In,Ga)Se_2$ Thin Films. *Sci. Rep.* **2017**, *7*, 41361−41367.
(19) Rusu, M.; Glatzel, Th.; Neisser, A.; Kaufmann, C. A.; Sadewasser, S.; Lux-Steiner, M. C. Formation of the Physical Vapor Deposited $CdS/Cu(In,Ga)Se_2$ Interface in Highly Efficient Thin Film Solar Cells. *Appl. Phys. Lett.* **2006**, *88*, 143510.
(20) Glatzel, Th.; Rusu, M.; Sadewasser, S.; Lux-Steiner, M. C. Surface Photovoltage Analysis of Thin CdS Layers on Polycrystalline Chalcopyrite Absorber Layers by Kelvin Probe Force Microscopy. *Nanotechnology* **2008**, *19*, 145705−145711.
(21) Jackson, P.; Hariskos, D.; Lotter, E.; Paetel, S.; Wuerz, R.; Menner, R.; Wischmann, W.; Powalla, M. New World Record Efficiency for $Cu(In,Ga)Se_2$ Thin-Film Solar Cells Beyond 20%. *Prog. Photovoltaics* **2011**, *19*, 894−897.
(22) Gorgoi, M.; Svensson, S.; Schäfers, F.; Öhrwall, G.; Mertin, M.; Bressler, P.; Karis, O.; Siegbahn, H.; Sandell, A.; Rensmo, H.; Doherty, W.; Jung, C.; Braun, W.; Eberhardt, W. The High Kinetic Energy Photoelectron Spectroscopy Facility at BESSY Progress and First Results. *Nucl. Instrum. Methods Phys. Res., Sect. A* **2009**, *601*, 48−53.
(23) Schaefers, F.; Mertin, M.; Gorgoi, M. KMC-1: A High Resolution and High Flux Soft X-ray Beamline at BESSY. *Rev. Sci. Instrum.* **2007**, *78*, 123102−123115.
(24) Seah, M. P.; Gilmore, I. S.; Spencer, S. J. XPS: Binding Energy Calibration of Electron Spectrometers 4-Assessment of Effects for Different X-Ray Sources, Analyser Resolutions Angles of Emission and Overall Uncertainties. *Surf. Interface Anal.* **1998**, *26*, 617−641.
(25) Jia, J. J.; Callcott, T. A.; Yurkas, J.; Ellis, A. W.; Himpsel, F. J.; Samant, M. J.; Stöhr, J.; Ederer, D. L.; Carlisle, A.; Hudson, E. A.; Terminello, L. J.; Shuh, D. K.; Perera, R. C. C. First Experimental Results from IBM/TENN/TULANE/LLNL/LBL Undulator Beamline at the Advanced Light Source. *Rev. Sci. Instrum.* **1995**, *66*, 1394−1397.
(26) Weinhardt, L.; Fuchs, O.; Umbach, E.; Heske, C.; Fleszar, A.; Hanke, W.; Denlinger, J. D. Resonant Inelastic Soft X-Ray Scattering, X-Ray Absorption Spectroscopy, and Density Functional Theory Calculations of the Electronic Bulk Band Structure of CdS. *Phys. Rev. B: Condens. Matter Mater. Phys.* **2007**, *75*, 165207.
(27) Sadewasser, S. Surface Potential of Chalcopyrite Films Measured by KPFM. *Phys. Status Solidi A* **2006**, *203*, 2571−2580.
(28) Handick, E.; Reinhard, P.; Wilks, R. G.; Pianezzi, F.; Kunze, T.; Kreikemeyer-Lorenzo, D.; Weinhardt, L.; Blum, M.; Yang, W.; Gorgoi, M.; Ikenaga, E.; Gerlach, D.; Ueda, S.; Yamashita, Y.; Chikyow, T.; Heske, C.; Buecheler, S.; Tiwari, A. N.; Bär, M. Formation of a K-In-Se Surface Species by NaF/KF Post-Deposition Treatment of $Cu(In,Ga)Se_2$ Thin-Film Solar Cell Absorbers. *ACS Appl. Mater. Interfaces* **2017**, *9*, 3581−3589.
(29) Tanuma, S.; Powell, C. J.; Penn, D. R. Calculations of Electron Inelastic Mean Free Paths. V. Data for 14 Organic Compounds Over the 50−2000 eV Range. *Surf. Interface Anal.* **1994**, *21*, 165−176.
(30) Shinotsuka, H.; Tanuma, S.; Powell, C. J.; Penn, D. R. Calculations of Electron Inelastic Mean Free Paths. X. Data for 41 Elemental Solids Over the 50 eV to 200 keV Range with the Relativistic Full Penn Algorithm. *Surf. Interface Anal.* **2015**, *47*, 871−888.
(31) Ballipinar, F.; Rastogi, A. C. High Transmittance Cadmium Oxysulfide Cd(S,O) Buffer Layer Grown by Triton X-100 Mediated Chemical Bath Deposition for Thin-Film Heterojunction Solar Cells. *J. Appl. Phys.* **2017**, *121*, 035302−035313.
(32) Meisel, A.; Leonhardt, G.; Szargan, R. *X-Ray Spectra and Chemical Binding*; Springer-Verlag: Berlin, 1989.
(33) Reichardt, J.; Bär, M.; Grimm, A.; Kötschau, I.; Lauermann, I.; Sokoll, S.; Lux-Steiner, M. C.; Fischer, Ch.-H.; Heske, C.; Weinhardt, L.; Fuchs, O.; Jung, Ch.; Gudat, W.; Niesen, T. P.; Karg, F. Inducing and Monitoring Photoelectrochemical Reactions at Surfaces and Buried Interfaces in $Cu(In,Ga)(S,Se)_2$ Thin-Film Solar Cells. *Appl. Phys. Lett.* **2005**, *86*, 172102−172104.
(34) Henke, B. L.; Gullikson, E. M.; Davis, J. C. X-Ray Interactions: Photoabsorption, Scattering, Transmission, and Reflection at E = 50−30,000 eV, Z = 1−92. *At. Data Nucl. Data Tables* **1993**, *54*, 181−342.
(35) Liao, D. Polar Surfaces of $Cu(In,Ga)Se_2$ Properties and Effects on Crystal Growth. PhD Thesis, University of Illinois, 2003.
(36) Bär, M.; Rusu, M.; Lehmann, S.; Schedel-Niedrig, T.; Lauermann, I.; Lux-Steiner, M. C. The Chemical and Electronic Surface and Interface Structure of $CuGaSe_2$ Thin-film Solar Cell Absorbers. *Appl. Phys. Lett.* **2008**, *93*, 232104−232106.

DOI: 10.1021/acsami.7b12448
ACS Appl. Mater. Interfaces 2017, 9, 44173−44180

(37) Lepetit, Th. Influence of KF Post Deposition Treatment on the Polycrystalline Cu(In,Ga)Se_2/CdS Heterojunction Formation for Photovoltaic Application. PhD Thesis, L'Université Nantes Angers Le Mans, 2015.
(38) Salomé, P. M. P.; Ribeiro-Andrade, R.; Teixeira, J. P.; Keller, J.; Törndahl, T.; Nicoara, N.; Edoff, M.; González, J. C.; Leitão, J. P.; Sadewasser, S. Cd and Cu Interdiffusion in Cu(In, Ga)Se_2/CdS Hetero-Interfaces. *IEEE Journal of Photovoltaics* **2017**, *7*, 858−863.

DOI: 10.1021/acsami.7b12448
ACS Appl. Mater. Interfaces 2017, 9, 44173−44180